ORIGINAL ARTICLE

Eco-friendly Fabrication of Gold Nanoparticles: Evaluation of Catalytic Dye Degradation and Antimicrobial Potential

Karthik Gunnam[1], Ajay Pujala[2], Nalayini J[3], Ponsankar A[4], Vanaja M[5], Sivakavinesan M[6]*

[1]Department of Forensic Medicine and Toxicology, Apollo Institute of Medical Sciences and Research, Dr NTR University, Chittoor, Andhra Pradesh, India, [2]Department of Anaesthesia, Saveetha Medical College and Hospital, Saveetha Institute of Medical and Technical Sciences (SIMATS), Saveetha University, Chennai, Tamil Nadu, India, [3]Department of Paediatrics, Saveetha Medical College and Hospital, Saveetha Institute of Medical and Technical Sciences (SIMATS), Saveetha University, Chennai, Tamil Nadu, India, [4]Department of Biotechnology, Sri Paramakalyani College, Manonmaniam Sundaranar University, Alwarkurichi, Tenkasi, Tamil Nadu, India, [5]Environmental Nanotechnology Lab, Saveetha Medical College and Hospital, Saveetha Institute of Medical and Technical Sciences, Chennai, Tamil Nadu, India, [6]Department of Chemistry, G. Venkataswamy Naidu College (Autonomous), Kovilpatti-628502. Tamil Nadu, India

Abstract

Background: Plant-derived and agricultural wastes constitute a major portion of global solid waste. Valorization of such biowastes offers a sustainable and eco-friendly approach for nanoparticle synthesis. **Aim:** This study aimed to green synthesize gold nanoparticles (AuNPs) using pomelo peel extract (PPE) and evaluate their photocatalytic dye degradation and antibacterial potential. **Methodology:** The AuNPs were bio-synthesized using optimal conditions (pH = 5, 1mM AuCl3, 10mg PPE, and 80°C). The produced nanoparticles were identified through UV-Visible (UV-VIS) spectroscopy, X-Ray Diffraction (XRD), Fourier Transform Infrared Spectroscopy (FTIR), Scanning Electron Microscopy (SEM), and Atomic Force Microscopy (AFM). Photocatalytic efficiency was examined using Methyl Red, Rhodamine B, and Quinoline Yellow in the presence of sunlight. Antibacterial effectiveness was tested using chosen Gram-positive and Gram-negative bacteria. **Results:** The UV-vis spectrum displayed an SPR peak of 525-550 nm. Crystalline nature was evidenced by X-ray diffraction of the planes (111), (200), and (220). Spherical polydisperse nanoparticles with 25-65 nm particle size were observed using SEM and AFM images. The presence of plant phytochemicals as reducers and stabilizers for gold nanoparticles was inferred from FTIR analysis. The synthesized gold nanoparticles showed high efficiency in dye degradation with percentage values of 84.78% (Methyl Red), 78.85% (Rhodamine B), and 82.16% (Quinoline Yellow) within 240 minutes, following pseudo first order kinetics. The synthesized AuNPs showed dose. **Conclusion:** The study demonstrates an eco-friendly and efficient approach for synthesizing AuNPs using pomelo peel waste, with promising applications in wastewater treatment and antibacterial therapy.

Key words: Antibacterial activity, biosynthesis, dye degradation, gold nanoparticles, photocatalysis, pomelo peel extract, reusability

INTRODUCTION

Nanotechnology has emerged as an effective platform for designing materials at the nanoscale level with diverse application. Physical, chemical, and biological methods have been developed for nanomaterial synthesis, and these materials find extensive applications across medicine, industry, and the environment. In recent years, a significant area of nanoscience study has been the integration of green chemistry ideas with nanotechnology.[1] Applications of nanomaterials in biomedicine and the environment are limited by the frequent production of toxic byproducts during the traditional chemical manufacturing process.[2] However, synthesis made possible by plant extract is regarded as an inexpensive and ecologically approachable process suitable for extensive production.[3,4] Gold nanoparticles (AuNPs) distinguish

Address for correspondence:
Dr. M. Sivakavinesan, M.Vanaja, Saveetha Medical College and Hospital, SIMATS -602 105, Tamil Nadu, India. E-mail: amvanaja@gmail.com

Received: 19-02-2026
Revised: 18-03-2026
Accepted: 27-03-2026

themselves from other noble metallic nanoparticles in a variety of applications, such as imaging, drug delivery, optics, catalysis, optoelectronics, diagnostics, microelectronics, and biological, chemical, and environmental sensing, because of their unique surface plasmon resonance (SPR) characteristics.[5,6] The manufacturing and characterization of noble metal nanoparticles is a well-established and respected topic of study. In this field, the choice of synthesis methods and subsequent applications continues to be the main drivers of ongoing research.[7-9]

The unique and tunable SPR properties of AuNPs have garnered significant attention in a number of biomedical applications, including drug delivery, tissue and carcinoma imaging, photothermal healing, and antibody-based pathogen detection in clinical specimens.[10-12] It is possible to create a wide range of forms, such as cubes, wires, octagons, triangles, rods, and hexagons, by carefully regulating their morphology with the choice of reducing agents.[13-16] Because of their gradual release of metal ions, which disrupts the metabolism of the microorganisms, metallic nanoparticles offer antibacterial properties in addition to these biological uses.[17] More research people are realizing that nanoparticles and nanocomposites are useful tools for addressing environmental problems outside of the biomedical industry.

Waste management is one of the main problems that agro-based businesses in developing countries face. Water bodies are contaminated by organic dyes found in the effluents discharged by the paper, textile, and pharmaceutical sectors.[18] Toxic dyes are removed from the polluted water using conventional methods, such as adsorption, photo-electric degradation, photocatalytic reduction, and microwave-aided degradation, which are effective but often energy-intensive and sometimes involve hazardous chemicals.[18-22] These limitations require sustainable procedures and materials that are green biosystems. Recent studies have demonstrated the potential use of plant-based nanomaterials in dye degradation.[23]

Pomelo (*Citrus maxima*), a citrus fruit widely cultivated in tropical regions, generates large quantities of peel waste. The peel is rich in essential oils, cellulose, tannins, coumarins, pectins, terpenes, and triterpenoids,[24,25] making it a potential resource for nanoparticle synthesis. The phytochemicals in pomelo peel act as natural reducing and stabilizing agents, while its valorization contributes to waste minimization and circular bioeconomy strategies.

In this study, pomelo peel was extracted with a suitable solvent and further used in the synthesis of AuNPs and characterized by using ultraviolet-vis (UV-vis) spectrophotometer, X-ray diffraction (XRD) studies, Fourier transform infrared (FTIR) spectroscopy, scanning electron microscope (SEM), and atomic force microscopy (AFM). The potential of these biosynthesized nanoparticles was used to degradation of industrial dyes are Methyl red, Rhodamine B, and Quinoline Yellow, under sunlight. In addition, the antibacterial effect of the nanoparticle is studied by testing against various pathogenic bacterial species are *Bacillus cereus, Bacillus subtilis, Pseudomonas aeruginosa,* and *Klebsiella pneumoniae.* This work is unique in that it uses pomelo peel extract (PPE) to systematically optimize the green fabrication of tiny gold particles, which are then used for both photocatalytic degradation of various industrial colors and antibacterial activity against important pathogens. Unlike prior works focused on other citrus peels, this research uniquely benchmarks three dyes under identical conditions and thoroughly reports kinetic data. The dual-functionality and sustainability aspect, using agricultural waste, make it distinct from existing studies.

MATERIALS AND METHODS

Materials used

B. cereus, *B. subtilis*, *Pseudomonas* spp., and *K. pneumoniae* strains were purchased from MTCC, IMTECH, Chandigarh. The Nutrient Agar and Muller-Hinton Agar medium used to grow and maintain the bacterial culture, hydrogen tetrachloroaurate (III) trihydrate, Acetone, rhodamine B, quinoline Y, and methyl red were obtained from Sri Ganapathy Scientifics, Srivilliputhur, India. The pomelo fruit peels were collected from the local market in Courtallam (8.9342°N 77.2778°E, MSL-167 m), Tenkasi, Tamil Nadu, India

Preparation of PPE

PPE was prepared according to the method described by Bankar *et al.*,[24] with minor modifications. The peels were then boiled in 100 mL of filtered water at 90°C for 30 min. After cooling, the boiled peels were manually crushed in 100 mL of distilled water, and the resulting mixture was filtered through a sterile muslin cloth. An equal volume of chilled acetone (1:1 ratio) was added to the filtrate to facilitate precipitation. The final precipitate was collected by centrifugation at 7000 rpm for 12 min. The pellet obtained was air-dried at room temperature to form a powder, which was stored in an air-tight container at room temperature and used for further experimental procedures.

Synthesis of AuNP

In this study, AuNPs s were synthesized under optimized conditions, which are 10 mg of PPE powder, 10 mL of 1 mM gold chloride solution (pH – 5), and heated at 80°C in a water bath shaker. The color conversion of the solution from light yellow to wine red represents the formation of AuNPs. To evaluate the favorable conditions for synthesizing nanoparticles, are followed by changing several parameters, such as the amount of PPE, the concentration of gold chloride solution, pH, and temperature. Changing the pH of the reaction mixtures (10 mg PPE, 1 mM gold chloride/10 mL) from 2.0 to 5.0 allowed

examining the impact of pH on nanoparticle production. To find the impact of the gold salt, the concentration of $HAuCl_4$ was increased from 0.125, 0.25, 0.5, and 1.0 mM, prepared in 10 mL of distilled water. The concentration of PPE was adjusted to 0.5, 1.0, 2.0, 4.0, and 10.0 mg while maintaining a concentration of 1 mM/10 mL of gold chloride. Temperature effects on nanoparticle production were investigated by incubating reaction solutions with 1 mM $HAuCl_4$, 10 mg PPE prepared in 10 mL, and a pH of 3.0 at 40, 60, 80, and 100°C. All the experiments are carried out under stirring conditions.

Characterization of AuNP

A UV-vis spectrophotometer (Perkin Elmer, Lambda 25) was used to characterize the produced AuNP. XRD was used to examine the crystalline structure of the produced AuNPs (Model: Diffractometer system XPERT-PRO). Using the Bruker TENSOR 27 FTIR model, the functional groups in the powdered PPE and AuNPs are examined. The morphological characteristics of the PPE-mediated AuNPs were analyzed using scanning electron microscopy (SEM; Tescan VEGA 3 SBH) and atomic force microscopy (AFM; Nanosurf EasyScan 2).

Dye removal application of AuNPs

Stock dye solutions were prepared by dissolving 1 mg of each dye in 100 mL of double-distilled water. For the photocatalytic experiments, 10 mg of green-synthesized AuNPs was added to 100 mL of each dye solution. To achieve adsorption–desorption equilibrium before being exposed to light, the solutions were agitated for 30 min using a magnetic stirrer. At specific time intervals, aliquots (2–3 mL) were withdrawn, filtered, and analyzed to monitor the degradation progress. The absorbance spectra of the filtrate were monitored using a UV-vis spectrophotometer in the wavelength range of 300–700 nm. Final concentration of the dye was determined by measuring absorbance at their respective maximum wavelengths (λ max): 555 nm for rhodamine B, 416 nm for quinoline yellow, and 410 nm for methyl red. Dye solution is considered as a control (without nanoparticles), and the degradation activity of nanoparticles was compared with PPE (without nanoparticles). The percentage of dye degradation was estimated by the following formula:

$$\% \text{ Dye removal} = \frac{I_c - F_c}{I_c} \times 100$$

Where, "I_C" and "F_C" are the initial and final concentration of dye solution before and after degradation by photocatalysis, respectively.

Anti-bacterial activity of AuNPs

Anti-bacterial activity of AuNP was assessed against bacterial strains of *P. aeruginosa*, *B. subtilis*, *K. pneumoniae*, and *B. cereus*. The antibacterial activity of AuNP against bacteria was tested by the agar-well diffusion method. Sterile Muller-Hinton agar medium was poured in culture plates, and the bacterial cultures (24 h culture) were swabbed onto the media by sterile cotton buds. About 5 wells were made with 6 mm was bored by using a cork-borer in the Muller-Hinton agar plates. Different concentrations of AuNPs (20, 40, 60, and 80 µg/mL) synthesized by using the peel extract powder are poured into the well by using a sterile micropipette; the control lacks the AuNPs and incubated at 35°C for 24 h. Zone formation around the well was measured after 24 h of incubation. The tests are repeated for three times for statistical assessment, and the data are expressed as mean ± standard error.

RESULTS AND DISCUSSION

Characterization of AuNPs

Optimization studies for synthesis of AuNPs using UV-vis spectrophotometer

Waste derived synthesis of AuNP was visually indicated by the changes in the solution color from yellow to purple pink due to the excitation of free electrons in the AuNPs, resulting in the SPR.[25] Figure 1 shows the UV-vis spectrum of AuNPs synthesized by peel extract powder. The spectra show a broad absorption band at 527 nm due to the SPR of the nanoparticles. This characteristic band obtained indicates the particles are larger in size and are polydispersed.[26,27] Various parameters are observed for nanoparticle synthesis, such as pH, gold ion concentration, PPE powder concentration, and temperature. Systematic optimization studies revealed that the formation of AuNP was strongly influenced by pH, gold ion concentration, PPE dosage, and temperature. pH is an important factor that affecting the functional group availability of plant extract and changes the output of the synthesized nanoparticles.[28]

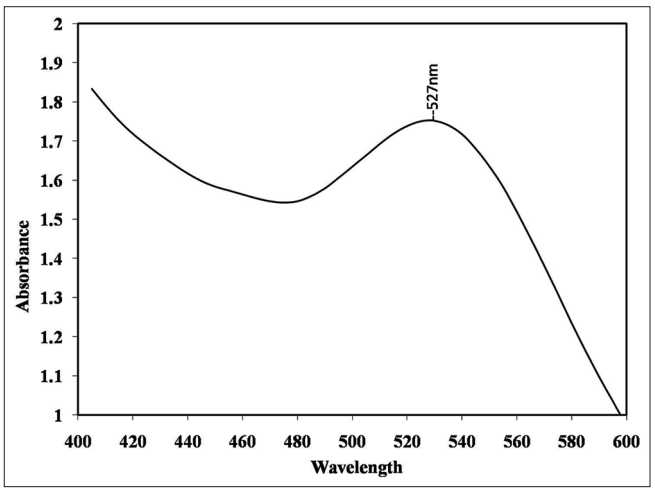

Figure 1: Ultraviolet-visible spectrum of gold nanoparticle showing surface plasmon resonance band at 527 nm

In this study, the effect of pH on the synthesis of nanoparticles is studied by varying the pH from 3 to 6, and the results are shown in Figure 2. The light-yellow color of the gold solution is changed to various colors and at higher pH, it is converted to maroon. The pH below 3 shows no SPR band, indicating the unavailability of functional biomolecules under acidic conditions. When the pH is increased gradually, the band is observed at 540 nm, and with further increase of pH, the band is positioned at 550–560 nm. The color intensity increases and produces a SPR band around 500–600 nm, indicating the production of AuNP. Moreover, optimal production of AuNPs was observed at pH 5 with a distinct SPR band range 540–550 nm, reliable with nucleation and growth of nanoparticles. Earlier studies stated that pH controls the synthesis, size, and stability of the nanoparticles. Very low pH suppresses the reduction process of metal ions into nanoparticles. Our results confirm that acidic pH hinders the formation of the nanoparticles, whereas moderate pH promotes the stability of the growth of nanoparticles. Moreover, lower pH enhances the formation of larger sizes of nanoparticles, whereas higher pH influences small-sized nanoparticle formation.[29,30]

Figure 3 shows the result of the concentration of gold ion on the synthesis of Au nanoparticles. Increasing gold ion concentration from 0.25 mM to 1 mM yielded sharp SPR bands at 540–550 nm range, while lower concentrations failed to initiate complete reduction. The solution displays different colors for 0.125 mM, 0.25 mM, 0.5 mM, and 1.0 mM gold ion concentrations, such as pale yellow, light brown, dark red, and purple red, respectively. 1.0 mM gold ion concentration treated with PPE extract shows a peak range 540–560 nm due to the anisotropic AuNP formation.[5,31] The morphological and distribution characters of nanoparticles were depended on the concentration of gold ions.[24,32,33]

The effect of PPE concentration (2.5, 5.0, 10, and 25 mg) on AuNP synthesis is shown in Figure 4. At lower concentrations (2.5 and 5.0 mg), no significant color change was observed, and no SPR band appeared in the UV-vis spectrum, indicating the absence of nanoparticle formation.[34,35] This is due to the insufficient amount of reducing agent, which leads to slower the reaction rate. In contrast, the reaction mixture containing 10 mg PPE displayed a distinct purple-pink coloration, along with a broad SPR band centered at 550 nm, suggesting effective nanoparticle synthesis. At 25 mg, a similar broad band was observed at 540 nm, although the particles were found to be poly-dispersed, likely due to an excess of phytochemicals that caused uncontrolled nucleation and aggregation.[34]

The influence of temperature on nanoparticle biosynthesis is shown in Figure 5. Reactions were carried out at different temperatures, such as 40, 60, 80, and 100°C. Among these, 80°C resulted in a characteristic purple–pink solution, suggesting it as the optimum temperature for AuNP synthesis. At 40 and 60°C, the reaction solution developed lighter red hues, while at 100°C, a darker red coloration was observed. The corresponding SPR bands were broadly distributed between 500 and 600 nm, consistent with the presence of large and

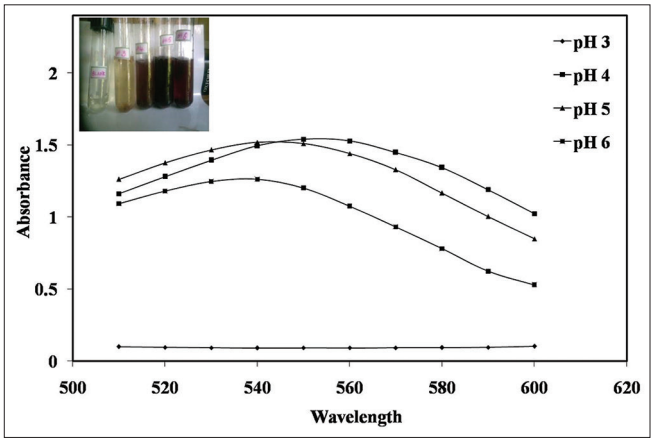

Figure 2: Ultraviolet-visible spectrum of the effect of pH on gold nanoparticle synthesis (inset figure shows the color change in the gold solution due to pH)

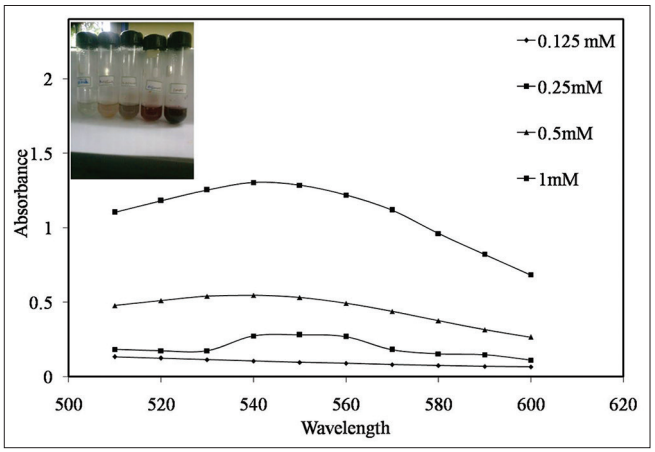

Figure 3: Ultraviolet-visible spectrum of the effect of gold concentration on gold nanoparticle synthesis (inset figure shows the color change in the gold solution due to gold concentration)

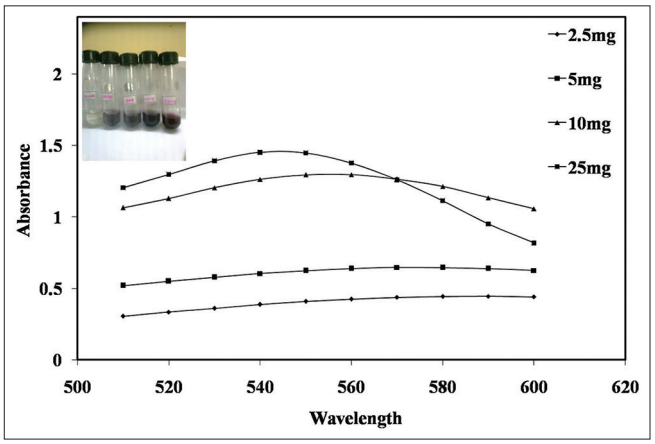

Figure 4: Ultraviolet-visible spectrum of the effect of pomelo peel extract (PPE) concentration on gold nanoparticle synthesis (inset figure shows the color change in gold solution due to PPE concentration)

poly-dispersed nanoparticles. The suboptimal temperatures may either slow the reduction rate (low temperatures) or induce excessive nucleation and growth (high temperatures). The shape and size of the nanoparticles can be controlled by temperature. Higher temperature speeds up the nanoparticles formation.[36-38] The optimized conditions for the production of AuNPs using PPE powder are summarized in Table 1.

XRD studies

Figure 6 indicates the XRD form of the AuNP synthesized using PPE. There are four different peaks found at 2θ values of 38.34°, 44.5°, 64.72°, and 77.84°, corresponding to the (111), (200), (220), and (311) planes of the crystalline AuNP (JCPDS card n. 04-0784)[39,40] and thus the crystallinity is confirmed with the size range from 20-46 nm. These features known to enhance electron transfer during photocatalysis. The unassigned peaks found at 2θ values of 28.45°, 40.64°, 50.23°, 66.45°, and 73.74° are due to the interferences present in the PPE, such as the terpenes or other biomolecules present in the peel extract.[41,42]

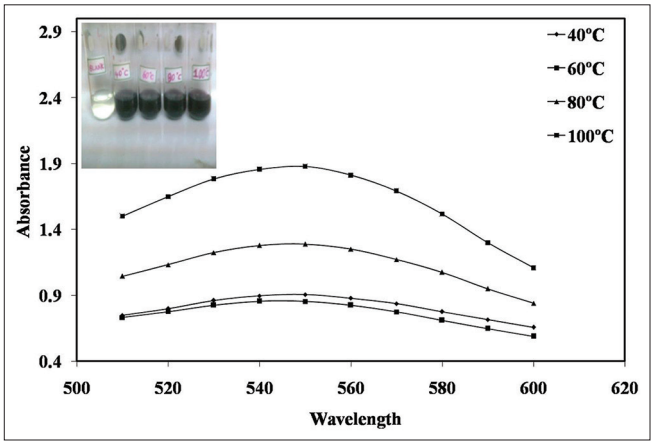

Figure 5: Ultraviolet-visible spectrum of the effect of temperature on gold nanoparticle synthesis (the inset figure shows the color change in gold solution due to temperature)

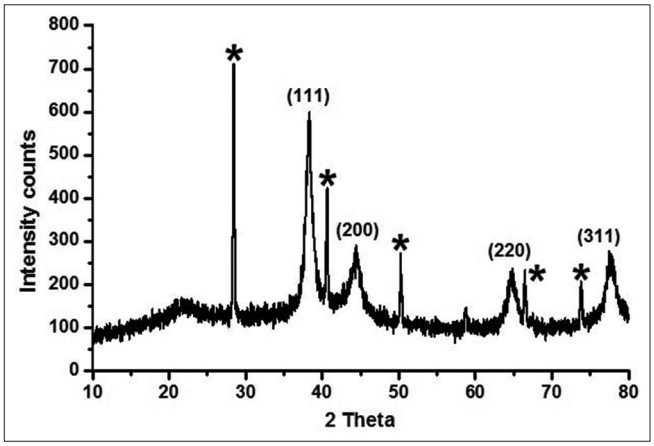

Figure 6: X-ray diffraction pattern of crystalline gold nanoparticle observed at 2 theta ranges from 10° to 80° shows different diffraction planes

Scanning electron microscopy (SEM)

SEM micrographs of a representative reaction mixture containing 10 mg of PPE powder and 1 mM gold chloride at pH 5 and PPE powder are shown in Figure 8. The SEM image displays that the particles are spherical in shape, with a size ranges from 25–67 nm and are well dispersed when seen at a distance of 2 μm and 1 μm.

Atomic force microscope

AFM, a bio-physical technique, is becoming important to study the morphology of nanoparticles and biomolecules.[43] The three-dimensional study of AuNP [Figure 9] shows the highly spherical nanoparticles at the scale ranging from (3–17 μm). Whereas Deshpande *et al.*[44] obtained irregular shaped AuNPs synthesized by using clove buds. Song *et al.*[45] obtained nanoplates synthesized out using *Magnolia kobus* and *Diopyros kaki* leaf extract.

FTIR analysis

FTIR spectroscopy investigation was carried out to identify the functional group existing in the synthesised nanoparticle. The FTIR spectrum of AuNP synthesized using PPE powder is shown in Figure 7. The absorption peaks are positioned at 3348, 2924, 2139, 1592, 1418, 1099, 673 cm^{-1}. The absorption peak at 3348 cm^{-1} correlates to the stretching vibrations of carboxylic acids, alcohols, and amino groups associated with flavonoids and phenols. The peak at 2924 cm^{-1} is due to the-OH stretch of acids present in the terpenoids. The-C≡C-stretch of alkynes is seen at 2139 cm^{-1}. The peak at 1592 cm^{-1} represents the –NH bending vibrations of amines or amides, especially associated with flavonoids and tannins. The peak detected at 1418 cm^{-1} is due to the –OH bend of acids. The absorbance peak at 1099 cm^{-1} is due to the –C-O-stretch of alcohols, anhydrides, and also due to the –C-O-C-stretch of ethers. Some amines also have stretching vibrations at 1099 cm^{-1}. The peak at 673 cm^{-1} arises due to the

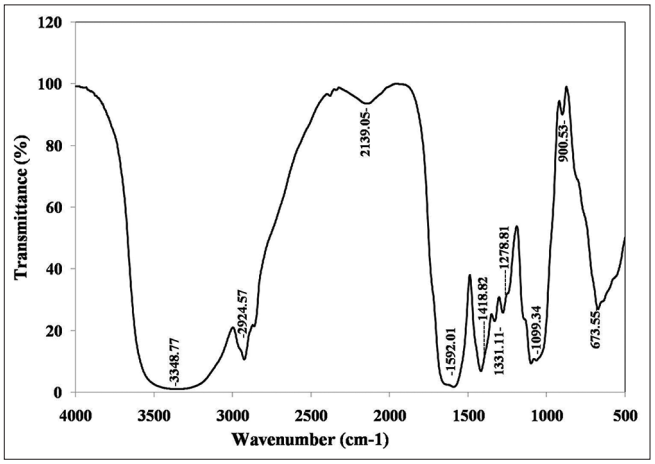

Figure 7: Fourier transform infrared spectra of gold nanoparticle shows functional groups recorded at different wavenumber region from 4000 cm^{-1} to 500 cm^{-1}

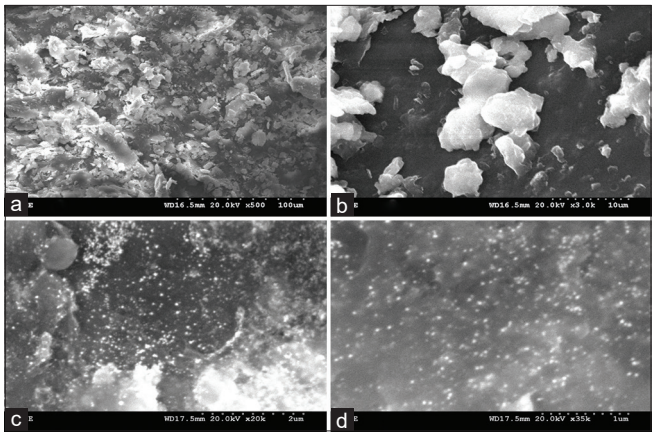

Figure 8: Scanning electron microscopy image of pomelo peel extract powder (a and b) and gold nanoparticle (c and d)

smaller quantities of impurities present due to the chloride contamination. The amine stretch is due to the proteins present in the extract, and the alcoholic and acidic stretching are due to bioactive compounds present in it. Collectively, the FTIR profiles support that phenolics, flavonoids, and tannins were responsible for the conversion of gold ion (Au^{3+}) into AuNPs, subsequently playing the dual role in reducing agent and stabilizing agent.

Photocatalytic degradation of dyes

Visual observation

Peel-mediated synthesized AuNP was treated against various dyes, such as methyl red, rhodamine B, and quinoline Y for studying their removal efficiency. The process was carried out under light. Color removal of the dyes by AuNPs is primarily identified by visually. The original color of the dyes was deep red, deep pink, and yellow for methyl red, rhodamine B, and quinoline Y, respectively, which were shown faded color after the incubation with AuNPs under light. Various color changes occur as corresponding to the incubation time. Finally, the complete removal of the color of the dyes was confirmed by the change of dye solution from colored to colorless.

UV-vis spectrophotometer

Degradation of methyl red

Methyl red degradation using AuNPs was carried out in different time intervals from 0 min to 24 h and confirmed by UV-vis spectrum. The UV-visible spectrum shows a characteristic peak at 410 nm for methyl red. The intensity of AuNPs treated dye was decreased as it increased with exposure time intervals. As decreasing the intensity of the dye and shows the increased peak ranges for AuNPs. The presence of an absorption peak at 540 nm was appeared and decreases the peak intensity of methyl red. The wide-ranging degradation of dye was noted with the disappearance of the

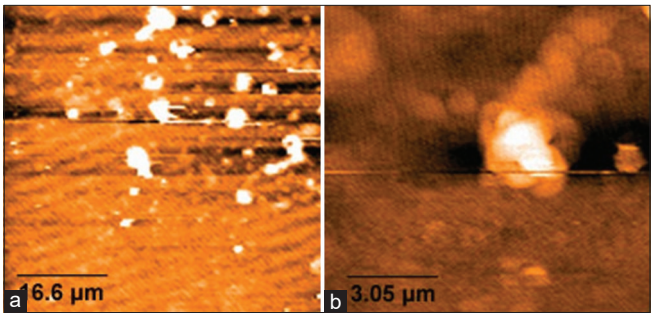

Figure 9: Atomic force microscopy image of gold nanoparticle (a) at 16.6 µm and (b) 3.05 µm

band for methyl red and the appearance of a typical SPR peak for AuNPs. This change was noted at the exposure time of 240 min [Figure 10a].

The photocatalytic dye removal of methyl red by AuNPs under the influence of sunlight was proved kinetically. The efficiency of AuNPs in dye degradation was examined by Co/Ct versus time (min) [Figure 10b], which showed gradually increase in degradation efficiency in dye concentration. This degradation fit with the pseudo-first-order model [Figure 10c] yielded a linear relationship between ln(Co/Ct) versus time with a correlation coefficient (R^2) of 0.91 with a rate constant (k) of 0.0079 min^{-1}. The percentage of methyl red degradation efficiency of peel-mediated synthesized AuNPs was calculated as 84.78% at the exposure time of 240 min under sunlight [Figure 10d and Table 2].

Degradation of Rhodamine B

The absorption band for Rhodamine B dye was placed at 555 nm, which is much closer to the SPR band of AuNPs. Hence, the dye degradation cannot be distinguished from the characteristic band of AuNP. However, a decrease in the intensity of the peak was observed due to the color removal as increase with exposing time, as shown in Figure 11a.

The efficiency of AuNPs in dye degradation was examined by Co/Ct versus time (min) [Figure 11b], which showed a gradual increase in the degradation of dye. The plot of Co/Ct versus time [Figure 11b] clearly depicts the continuous reduction in concentration of the rhodamine dye as the reaction progresses, with a sharp increase after 180 min, confirming enhanced degradation efficiency at longer exposure times. The kinetic study [Figure 11c] follows a pseudo-first-order model, as demonstrated by the linear relationship of ln(Co/Ct) versus time with a high regression coefficient ($R^2 = 0.946$), confirming that the degradation process obeys pseudo-first-order kinetics. The rate constant for the reaction is given by the slope of the fitted line. Furthermore, the percentage of degradation of dye using AuNPs is to be 78.40% at the exposing time of 240 min, as shown in Figure 11d and Table 2. Similarly, Arunachalam *et al.*[46] demonstrated the photocatalytic degradation of coomassie brilliant blue by using silver nanoparticles.

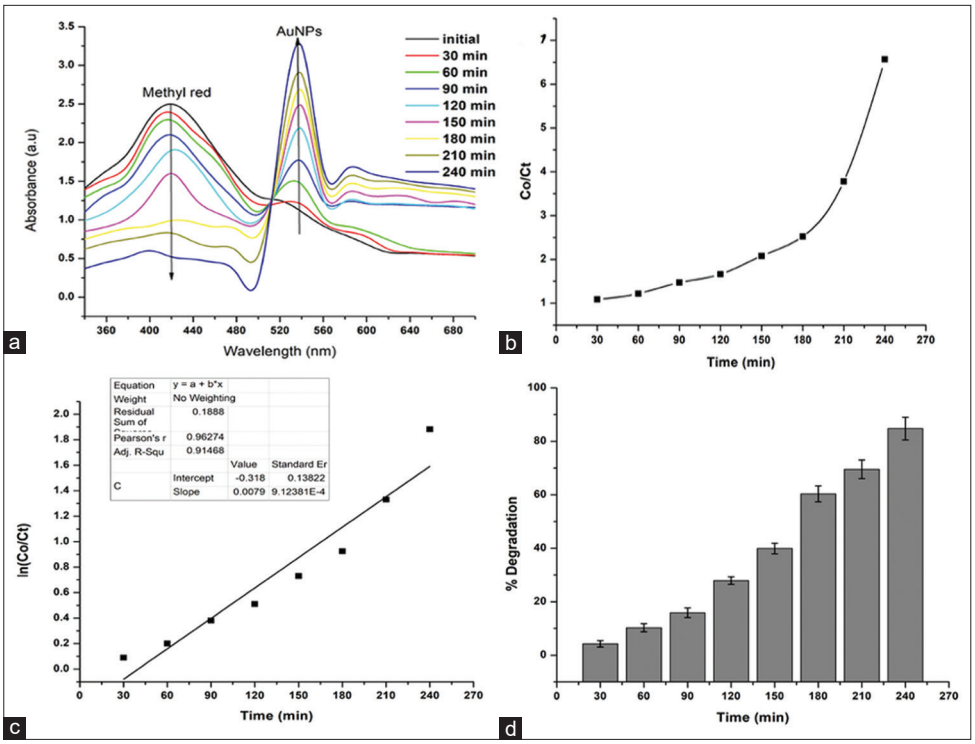

Figure 10: (a) Ultraviolet-visible absorption spectra of methyl red (MR) recorded at different irradiation times (0–240 min), showing a gradual decrease in the characteristic absorption peak, confirming effective photocatalytic degradation by gold nanoparticles. (b) Plot of concentration ratio (C/C_0) of MR dye with irradiation time. (c) Pseudo-first-order kinetic plot of $\ln(C_0/C)$ versus irradiation time. (d) Percentage degradation of the MR dye

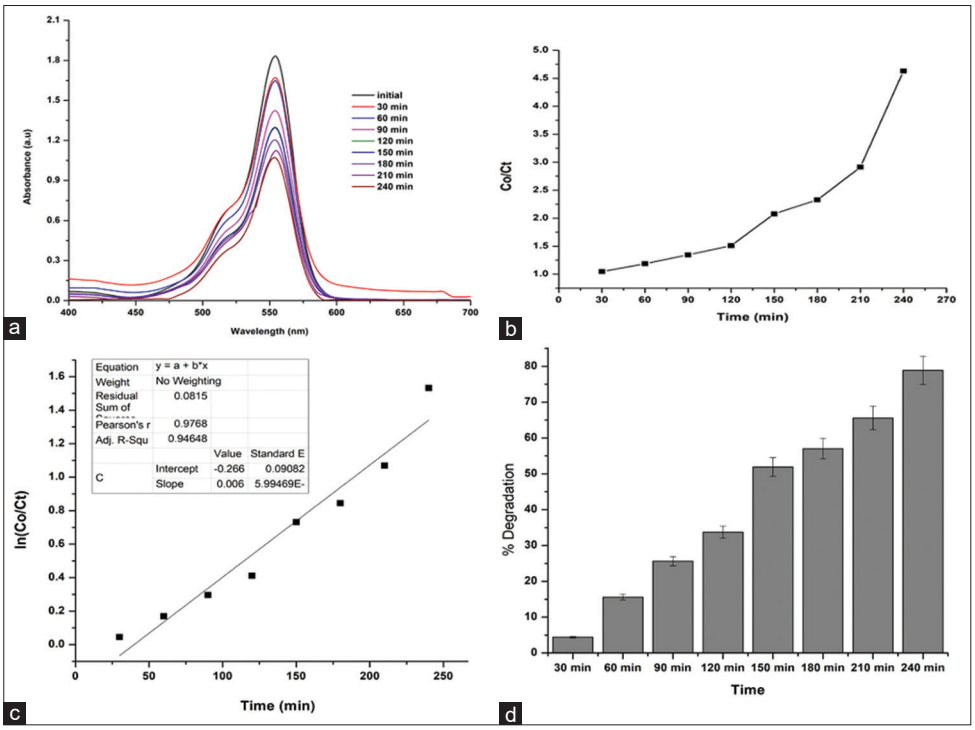

Figure 11: (a) Ultraviolet-visible absorption spectra of Rhodamine B (RB) recorded at different irradiation times (0–240 min), showing a gradual decrease in the characteristic absorption peak, confirming effective photocatalytic degradation by gold nanoparticles. (b) Plot of concentration ratio (C/C□) of rhodamine dye with irradiation time. (c) Pseudo-first-order kinetic plot of ln(C□/C) versus irradiation time. (d) Percentage degradation of rhodamine dye

Degradation of Quinoline Y

The degradation of quinoline Y treated with AuNPs was analyzed at different exposure times under sunlight. Initially, the maximum peak of quinoline Y in the UV-Vis spectrum was observed at 416 nm. This peak intensity was gradually decreased with increased exposure time up to 240 min, and appeared a characteristic peak at 540 nm for AuNPs. It indicates that the degradation or removal of dye by the action of AuNPs [Figure 12a]. The Co/Ct versus time plot [Figure 12b] illustrates the decrease in dye concentration over time, with a noticeable acceleration in degradation after 180 min, suggesting enhanced catalytic activity at prolonged exposure. The linear fit of ln(Co/Ct) versus time with a significant correlation coefficient ($R^2 = 0.925$) in the kinetic study [Figure 12c] further validates the pseudo-first-order behavior and suggests that the deterioration follows a pseudo-first-order kinetic model. The plot's slope indicates the reaction's rate constant. The percentage degradation plot [Figure 12d] demonstrates a steady increase in removal efficiency, reaching more than 82.16% degradation at 240 min. Overall, these findings confirm that AuNPs act as an effective photocatalyst for Quinoline Yellow dye removal, with efficiency increasing over time and the process governed by pseudo-first-order kinetics.

Comparison with control experiments

The comparative degradation efficiencies of Methyl Red, Rhodamine B, and Quinoline Yellow under different conditions are shown in the bar graph. In the absence of photocatalysts, only sunlight exposure resulted in negligible degradation of all dyes, indicating their high stability under natural light alone. When dyes were treated with plant extract (PPE) under light, moderate degradation was observed (about 50–60%), suggesting that the bioactive compounds in PPE play a major role in dye breakdown. In the presence of AuNPs under dark conditions, a limited extent of degradation occurred (15–30%), which may be attributed to the adsorption of dye molecules on the nanoparticle surface rather than photocatalysis. However, the combination of AuNPs with sunlight resulted in the highest degradation efficiency, exceeding 80% for all three dyes, confirming the strong photocatalytic activity of AuNPs under solar irradiation. Among the dyes, Methyl Red exhibited slightly higher degradation compared to Rhodamine B and Quinoline Yellow, but all three showed significant removal under the optimized condition (AuNPs + sunlight). This clearly demonstrates that AuNPs are highly effective photocatalysts, with sunlight irradiation greatly enhancing their performance in dye degradation. The comparative degradation efficiencies under different experimental conditions are presented in Figure 13, clearly demonstrating the superior photocatalytic performance of AuNPs under sunlight. The stability and reusability of the synthesized AuNPs were evaluated over multiple catalytic cycles, and the results indicate only a slight decrease in degradation efficiency, confirming good recyclability [Figures 14 and 15].

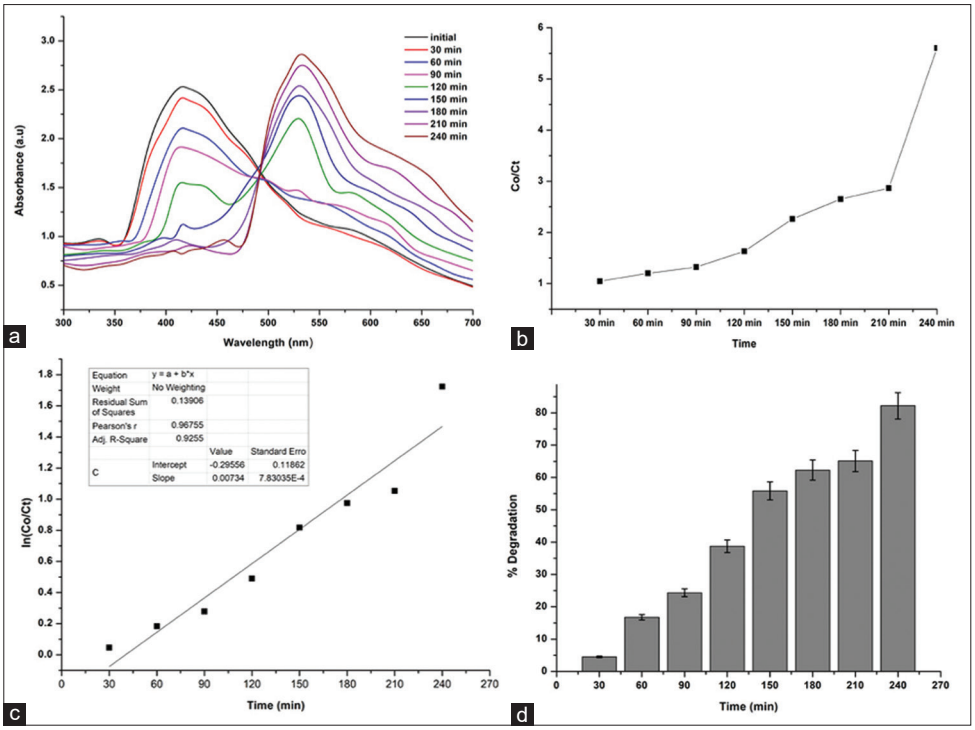

Figure 12: (a) Ultraviolet-visible absorption spectra of Quinoline Y (QY) recorded at different irradiation times (0–240 min), showing a gradual decrease in the characteristic absorption peak, confirming effective photocatalytic degradation by gold nanoparticles. (b) Plot of concentration ratio (C/C_0) of QY dye with irradiation time. (c) Pseudo-first-order kinetic plot of $\ln(C_0/C)$ versus irradiation time. (d) Percentage degradation of QY dye

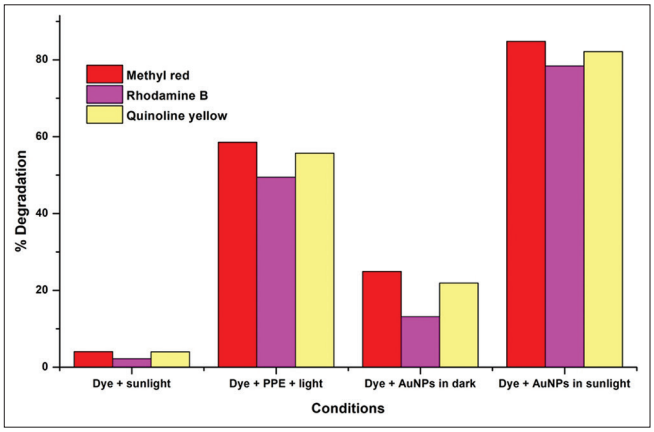

Figure 13: Comparative degradation efficiency of 3 dyes under different treatment conditions: (i) Dye exposed to sunlight alone, (ii) dye treated with plant peel extract under light, (iii) dye treated with gold nanoparticles (AuNPs) in the dark, and (iv) dye treated with AuNPs under sunlight. The results show enhanced degradation in the presence of AuNPs, particularly under sunlight irradiation

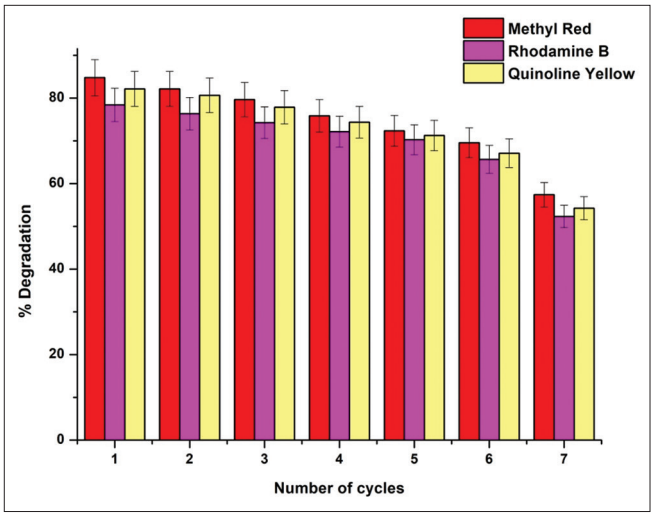

Figure 14: Reusability of gold nanoparticles for dye degradation over multiple cycles. Percentage degradation of methyl red, Rhodamine B, and Quinoline Yellow over seven consecutive catalytic cycles

Although a complete mechanism for the degradation of dyes by nanoparticles is still not fully known, several hypotheses have been forwarded. On exposure to sunlight, the localized SPR of AuNPs becomes excited, and collective oscillations arise in conduction electrons. The energy from these oscillations decays non-radiatively with the subsequent production of energetic hot electrons and holes. These hot electrons are shifted to AuNPs, which contain adsorbed oxygen molecules and generate reactive oxygen species (ROS), such as superoxide (O_2^-), hydroxyl (-OH), and hydrogen peroxide (H_2O_2). While the holes oxidize adsorbed water molecules into hydroxyl radicals, and these radicals are actively degrading dye molecules into smaller intermediates and eventually convert them into CO_2, H_2O, and inorganic ions.[21,22] The efficiency of the process could be limited by the recombination of charge carriers and an insufficient amount of oxygen/water acting as electron/hole acceptors. Effective dye adsorption on the nanoparticle surface and efficient charge separation enhance the degradation rate.[23,42,44]

Anti-bacterial activity

In addition to various applications of AuNPs the antibacterial activity is considered as most important application. The antibacterial activity is investigated with the PPE mediated AuNPs. Peel-mediated synthesized AuNPs exhibit excellent antibacterial activity was determined by agar well diffusion method against *B. subtilis*, *K. pneumoniae*, *P. aeruginosa,* and *B. cereus* at different concentrations 20, 40, 60, and 80 µg/mL [Table 3]. In this study, as the concentrations of AuNPs increases, such as 20, 40, 60, and 80 µg/mL, the zone formation also increased. The highest zone formation was observed against *K. pneumoniae* and *P. aeruginosa*.

AuNPs show a higher growth-retarding effect against Gram-negative (G^{-ve}) bacteria than the Gram-positive (G^{+ve}) bacteria; this variation in inhibition is due to the difference in the composition of the cell membrane of the bacteria. Gram-positive bacteria have a thick cell wall and complex composition, whereas Gram-negative bacteria have a thin cell wall, so the

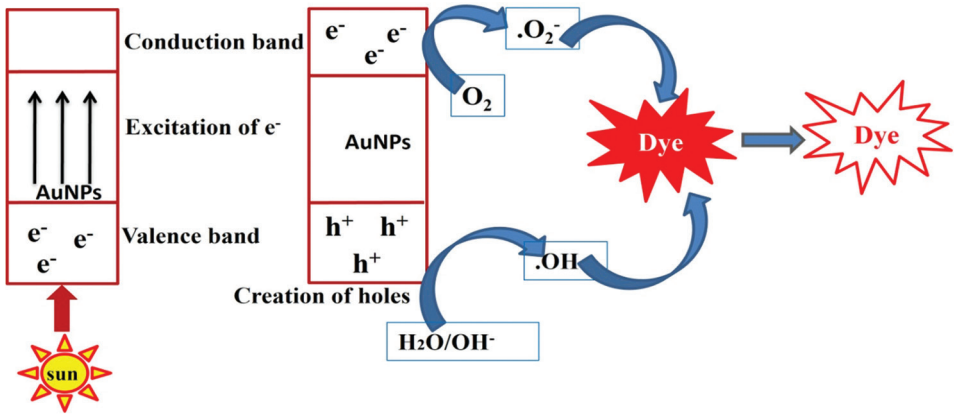

Figure 15: Possible mechanism of photocatalytic degradation of dye molecules by gold nanoparticles under sunlight

Table 1: Optimized conditions for the production of gold nanoparticles using PPE powder

Parameter	Range studied	Observed color change	SPR band (nm)	Inference/Outcome
pH	3–6	Light yellow→maroon (at higher pH)	Absent (<pH 3); 540–560 nm (pH 4–6)	pH <3: No reduction (no SPR); pH 5 optimal→distinct SPR at 540–550 nm with controlled nucleation
Gold ion concentration	0.125–1.0 mM	Pale yellow→light brown→dark red→purple red	540–550 nm (≥0.25 mM)	<0.25 mM: Incomplete reduction; ≥0.5 mM: effective nanoparticle formation, 1 mM optimal
PPE concentration	2.5, 5.0, 10, 25 mg	No change (2.5, 5.0 mg) → purple pink (10 mg) → purple red (25 mg)	None (2.5, 5.0 mg); 550 nm (10 mg); 540 nm (25 mg)	10 mg optimal; 25 mg caused polydispersity due to excess phytochemicals
Temperature	40, 60, 80, 100°C	Light red (40–60°C) → purple pink (80°C) → dark red (100°C)	Broad 500–600 nm	80°C optimal; low temp=Slow reduction, high temp=Uncontrolled nucleation/aggregation

PPE: Pomelo peel extract

Table 2: Degradation percentage of dyes by gold nanoparticles

Incubation	% dye degradation		
	Methyl red	Rhodamine B	Quinoline Y
30 min	05.49	04.41	04.52
60 min	10.26	15.59	16.74
90 min	15.87	25.61	24.33
120 min	27.89	33.73	38.72
150 min	50.52	51.89	55.84
180 min	60.34	57.03	62.28
210 min	69.55	65.67	65.11
240 min	84.78	78.40	82.16

Table 3: Anti-bacterial activity of gold nanoparticles against *B. cereus, K. pneumoniae, B. subtilis,* and *P. aeruginosa*

Organism/Dosage	Zone of inhibition (mm in diameter)			
	20 µg/mL	40 µg/mL	80 µg/mL	Antibiotic (10 mcg)
B. subtilis	05.83±0.44	06.97±0.33	07.17±0.44	12.50±0.33
K. pneumonia	08.50±0.29	09.33±0.44	11.33±0.33	14.00±0.51
P. aeruginosa	09.17±0.17	11.10±0.49	13.50±0.29	16.50±0.33
B. cereus	05.50±0.29	05.83±0.17	06.24±0.37	13.50±0.29

B. cereus: *Bacillus cereus*, *K. pneumonia: Klebsiella pneumoniae*, *B. subtilis: Bacillus subtilis*, *P. aeruginosa: Pseudomonas aeruginosa*

AuNPs easily penetrate into the cell in the form of ions and causes severe damages. This bacterial growth inhibition was occurred by nanoparticles, causing several damages, such as changing the property and potential of the cell membrane, hindering the activity of ATP, and affects the binding mechanism of ribosomal subunits.[47-49] Some of the studies revealed that AuNP possesses low toxicity to mammalian cells, and also the toxicity depends on the size and dosage of the nanoparticles. Lower dosage and smaller size of the nanoparticles cause minimal effects, while higher dosages cause severe effects, such as decreased survival rate, developmental abnormalities of cells, and oxidative stress.[50,51] Hence, the bioAuNPs can be used to remove toxic dyes in the environment without causing any hazard to the microflora in the aquatic system.

CONCLUSION

The AuNPs are synthesized using PPE powder. The method is a simple and low-cost method. Since only the solid waste is used as the substrate for synthesizing, the hazardous effects of chemicals and exploiting of plant materials are reduced to a larger extent. This method also recycles the agricultural waste and reduces the solid waste generation. The characterization of the synthesized PPE-AuNPs was

done by UV-vis spectroscopy, FTIR, XRD, SEM, and AFM. The AuNPs synthesized are spherical in shape, and the same was established by the SEM analysis. Thus, synthesized and characterized AuNPs are used for the degradation of industrially important dyes, such as methyl red, rhodamine B, and quinoline yellow. The industrial dyes are degraded by PPE-AuNPs in the presence of light to a greater extent. The AuNPs are tested for antibacterial activity against various bacterial strains compared with the control. The results concluded that these synthesized AuNPs have the ability to degrade industrial dyes and bactericidal effects. Thus, the particles can be used for dye degradation without any harm to the microorganism in the aquatic system. Moreover, the pomelo peel-mediated synthesis is a greener method for the synthesis of AuNPs.

CONFLICT OF INTEREST

The authors declare no competing interests.

ETHICAL APPROVAL

Not applicable.

REFERENCES

1. Philip D, Unni C. Extracellular biosynthesis of gold and silver nanoparticles using *Krishna tulsi* (*Ocimum sanctum*) leaf. Physica E Low Dimens Syst Nanostructure 2011;43:1318-22.
2. Philip D. Honey mediated green synthesis of gold nanoparticles. Spectrochim Acta Part a Mol Biomol Spectrosc 2009;73:650-3.
3. Sastry M, Ahmad A, Khan MI, Kumar R. Biosynthesis of metal nanoparticles using fungi and *Actinomycete*. Curr Sci 2003;85:162-70.
4. Vankar PS, Bajpai D. Preparation of gold nanoparticles from *Mirabilis jalapa* flowers. Indian J Biochem Biophys 2010;47:157-60.
5. Kelly KL, Coronado E, Zhao LL, Schatz GC. The optical properties of metal nanoparticles: The influence of size, shape, and dielectric environment. J Phys Chem B 2003;107:668-77.
6. Malarkodi C, Rajeshkumar S, Annadurai G. Detection of environmentally hazardous pesticide in fruit and vegetable samples using gold nanoparticles. Food Control 2017;80:11-8.
7. Sau TK, Rogach AL, Jackel F, Klar TL, Feldmann J. Properties and applications of colloidal nonspherical noble metal nanoparticles. Adv Mater 2010;22:1805-25.
8. Rajeshkumar S. Green synthesis of different sized antimicrobial silver nanoparticles using different parts of plants-a review. Int J ChemTech Res 2016;19:197-208.
9. Keerthiga N, Anitha R, Rajeshkumar S, Lakshmi T. Antioxidant activity of cumin oil mediated silver nanoparticles. Pharmacogn J 2019;11:787-9.
10. El-Sayed MA. Some interesting properties of metals confined in time and nanometer space of different shape. Acc Chem Res 2001;34:257-64.
11. Huang SH. Gold nanoparticle-based immunochromatographic test for identification of *Staphylococcus aureus* from clinical specimens. Clin Chim Acta 2006;373:139-43.
12. Narayanan KB, Sakthivel N. *Coriander* leaf mediated biosynthesis of gold nanoparticles. Mater Lett 2008;62:4588-90.
13. Jana NR, Gearheart L, Murphy CJ. Seed-mediated growth approach for shape-controlled synthesis of spheroidal and rod-like gold nanoparticle using a surfactant template. Adv Mater 2001;13:1389-93.
14. Wang L, Chen X, Zhan J, Chai Y, Yang C, Xu L, *et al*. Synthesis of gold nano-and microplates in hexagonal liquid crystals. J Phys Chem B 2005;109:3189-94.
15. Seo D, Park C, Song H. Polyhedral gold nanocrystals with O_h symmetry: From octahedra to cubes. J Am Chem Soc 2006;128:14863-70.
16. Pazos-Pe'rez N, Baranov D, Irsen S, Hilgendorff M, Liz-Marza'n LM, Giersig M. Synthesis of flexible, ultrathin gold nanowires in organic media. Langmuir 2008;24:9855-60.
17. Al-Ardi MH. The uses of gold nanoparticles and *Citrullus colocynthis* L. nanoparticles against of *Giardia lamblia in vivo*. Clin Epidemiol Glob Health 2020;8:1282-6.
18. Zaharia A, Suteu D. Textile organic dyes-characteristics, polluting effects and separation/elimination procedures from industrial effluents-a critical overview. In: Puzyn T, editor. Organic Pollutants Ten Years after the Stockholm Convention-Environmental and Analytical Update. London: InTechOpen; 2012.
19. Safarik I, Ptackova L, Safarikova M. Adsorption of dyes on magnetically labeled baker's yeast cells. Eur Cells Mater 2002;3:52-5.
20. Bo LL, Zhang YB, Quan X, Zhao B. Microwave assisted catalytic oxidation of p-nitrophenol in aqueous solution using carbon-supported copper catalyst. J Hazard Mater 2008;153:1201-6.
21. Lin J, Zong R, Zhou M, Zhu Y. Photoelectric catalytic degradation of methylene blue by C60-modified TiO_2 nanotube array. Appl Catal Environ 2009;89:425-31.
22. Pajootan E, Arami M, Rahimdokht M. Application of carbon nanotubes coated electrodes and immobilized TiO_2 for dye degradation in a continuous photocatalytic-electro-fenton process. Ind Eng Chem Res 2014;53:16261-9.
23. Baruah D, Goswami M, Yadav RN, Yadav A, Das AM. Biogenic synthesis of gold nanoparticles and their application in photocatalytic degradation of toxic dyes. J Photochem Photobiol B Biol 2018;186:51-8.
24. Bankar A, Joshi B, Kumar AR, Zinjarde S. Banana peel extract mediated synthesis of gold nanoparticles.

Colloids Surf B Biointerfaces 2010;80:45-50.
25. Mulvaney P. Surface plasmon spectroscopy of nanosized metal particles. Langmuir 1996;12:788-800.
26. Haiss W, Thanh NT, Aveyard J, Fernig DG. Determination of size and concentration of gold nanoparticles from UV-Vis spectra. Anal Chem 2007;79:4215-21.
27. Shalini C, Kowsaliya E, Malakondaiah S, Ramesh Babu PB, Jothinathan MK, Visuvasam MR. Physicochemical analysis of green synthesis gold nanoparticles of edible plant extracts. Res J Pharm Technol 2025;18:1739-2.
28. Enayati Ahangar L, Movassaghi K, Yaghoobi F. The pH role in nanotechnology, electrochemistry, and nano-drug delivery. Iran J Chem Chem Eng 2002;41:2175-88.
29. El-Kassas HY, El-Sheekh MM. Cytotoxic activity of biosynthesized gold nanoparticles with an extract of the red seaweed *Corallina officinalis* on the MCF-7 human breast cancer cell line. Asian Pac J Can Prevent 2014;15:4311-7.
30. Yang B, Qi F, Tan J, Yu T, Qu C. Study of green synthesis of ultrasmall gold nanoparticles using *Citrus sinensis* Peel. Appl Sci 2019;9:2423.
31. Ahmad T, Wani IA, Ahmed J, Al-Hartomy OA. Effect of gold ion concentration on size and properties of gold nanoparticles in TritonX-100 based inverse microemulsions. Appl Nanosci 2014;4:491-8.
32. Yasmin A, Ramesh K, Rajeshkumar S. Optimization and stabilization of gold nanoparticles by using herbal plant extract with microwave heating. Nano Converg 2014;1:12.
33. Bano A, Dawood A, Saira F, Malik A, Alkholief M, Ahmad H, *et al*. Enhancing catalytic activity of gold nanoparticles in a standard redox reaction by investigating the impact of AuNPs size, temperature and reductant concentrations. Sci Rep 2023;13:12359.
34. Kim HS, Seo YS, Kim K, Han JW, Park Y, Cho S. Concentration effect of reducing agents on green synthesis of gold nanoparticles: Size, morphology, and growth mechanism. Nanoscale Res Lett 2016;11:230.
35. Yoo S, Nam DH, Singh TI, Leem G, Lee S. Effect of reducing agents on the synthesis of anisotropic gold nanoparticles. Nano Convergence 2022;9:5.
36. Dutta A, Paul A, Chattopadhyay A. The effect of temperature on the aggregation kinetics of partially bare gold nanoparticles. RSC Adv 2016;6:82138-49.
37. Hammami I, Alabdallah NM, Al Jomaa A, Kamoun M. Gold nanoparticles: Synthesis properties and applications. J King Saud Univ Sci 2021;c33:101560.
38. Mountrichas G, Pispas S, Kamitsos EI. Effect of temperature on the direct synthesis of gold nanoparticles mediated by poly(dimethylaminoethyl methacrylate) homopolymer. J Phys Chem C 2014;11:22754-9.
39. Krishnamurthy S, Esterle A, Sharma NC, Sahi SV. Yucca-derived synthesis of gold nanomaterial and their catalytic potential. Nanoscale Res Lett 2014;9:627.
40. Alharbi NS, Bhakyaraj K, Gopinath K, Govindarajan M, Kumuraguru S, Mohan S, *et al*. Gum-mediated fabrication of eco-friendly gold nanoparticles promoting cell division and pollen germination in plant cells. J Clust Sci 2017;28:507-17.
41. Kalishwaralal K, Deepak V, Ram Kumar PS, Kottaisamy M, BarathmaniKanth S, Kartikeyan B, *et al*. Biosynthesis of silver and gold nanoparticles using *Brevibacterium casei*. Colloids Surf B Biointerfaces 2010;77:257-62.
42. Nayak S, Sajankila SP, Vaman Rao C. Green synthesis of gold nanoparticles from banana pith extract and its evaluation of antibacterial activity and catalytic reduction of malachite green dye. J Microbiol Biotechnol Food Sci 2018;7:641-5.
43. Best RB, Brockwell DJ, Toca-Herrera JL, Blake AW, Smith DA, Radford SE, *et al*. Force mode atomic force microscopy as a tool for protein folding studies. Anal Chim Acta 2003;479:87-105.
44. Deshpande R, Bedre MD, Basavaraja S, Sawle B, Manjunath SY, Venkataraman A. Rapid biosynthesis of irregular shaped gold nanoparticles from macerated aqueous extracellular dried clove buds (*Syzygium aromaticum*) solution. Colloids Surf B Biointerfaces 2010;79:235-40.
45. Song JY, Jang HK, Kim BS. Biological synthesis of gold nanoparticles using *Magnolia kobus* and *Diopyros kaki* leaf extracts. Process Biochem 2009;44:1133-8.
46. Arunachalam R, Dhanasingh S, Kalimuthu B, Uthirappan M, Rose C, Mandal AB. Phytosynthesis of silver nanoparticles using *Coccinia grandis* leaf extract and its application in the photocatalytic degradation. Colloids Surf B Biointerfaces 2012;94:226-30.
47. Dror-Ehre A, Mamane H, Belenkova T, Markovich G, Adin A. Silver nanoparticle-*E. Coli* colloidal interaction in water and effect on *E. Coli* survival. J Colloid Interface Sci 2009;339:521-6.
48. Dharman S, Maragathavalli G, Shanmugam R, Shanmugasundaram K. Curcumin mediated gold nanoparticles and analysis of its antioxidant, anti-inflammatory, antimicrobial activity against oral pathogens. Pesqui Brasil Odontopediatr Clín Integr 2023;23:e220068.
49. Viswanathan S, Palaniyandi T, Kannaki P, Shanmugam R, Baskar G, Rahaman AM, *et al*. Biogenic synthesis of gold nanoparticles using red seaweed *Champia parvula* and its anti-oxidant and anticarcinogenic activity on lung cancer. Partic Sci Technol 2023;41:241-9.
50. Aljohani FS, Hamed MT, Bakr BA, Shahin YH, Abu-Serie MM, Awaad AK, *et al*. *In vivo* bio-distribution and acute toxicity evaluation of greenly synthesized ultra-small gold nanoparticles with different biological activities. Sci Rep 2022;12:6269.
51. Arroyo G, Toscano F, Angulo Y, Arias MT, Stael C, Soria J, *et al*. Green synthesis of antioxidant and low-toxicity gold and silver nanoparticles using floral extracts. Open Nano 2025;26:100258.

Source of Support: Nil. **Conflicts of Interest:** None declared.